Carbon Nanotube—MoS_2 Composites as Solid Lubricants

Xianfeng Zhang,[†] Brandon Luster,[†] Amelia Church,[†] Christopher Muratore,[‡] Andrey A. Voevodin,[‡] Punit Kohli,[*,§] Samir Aouadi,[*,†] and Saikat Talapatra[*,†]

Departments of Physics and of Chemistry and Biochemistry, Southern Illinois University—Carbondale (SIUC), Carbondale, Illinois 62901, and Air Force Research Laboratory, Materials and Manufacturing Directorate, Wright-Patterson Air Force Base, Ohio 45433

ABSTRACT Solid lubricants (SLs) characterized by low coefficients of friction (μ) and wear rates (w) drastically improve the life span of instruments that undergo extreme frictional wear. However, the performance of SLs such as sputtered or nanoparticulate molybdenum disulfide (MoS_2), tungsten disulfide (WS_2), or graphite deteriorates heavily under extreme operational conditions such as elevated temperatures and high humidity. Here, we present our preliminary results, which demonstrate that composites of carbon nanotubes (CNTs) and MoS_2 produced by electrodeposition of MoS_2 on vertically aligned CNT films have low μ (~0.03) and w ($\sim 10^{-13}$ mm^3/N · mm) even at 300 °C, which are about 2 orders of magnitude better than those of nanoparticulate MoS_2-based coatings. The high load-bearing capacity of CNTs provides a strong enduring support to MoS_2 nanoclusters and is responsible for their ultralow w. The incorporation of these composites in liquid lubricants reduces the friction coefficient of the liquid lubricants by ~15%. The technique described here to produce SL coatings with extremely appealing frictional properties will provide valuable solutions for a variety of tribological applications where the coatings encounter high temperature, reduced pressure, and/or low- and high-humidity conditions.

KEYWORDS: solid lubricants • nanocomposites • carbon nanotubes • tribology • wear

INTRODUCTION

Solid lubricants (SLs) are used in extreme conditions that include low/high temperature, high radiation, high vacuum, and humidity (1—7). Transition-metal dichalcogenides such as MoS_2 (1), WS_2 (2), and graphite (4) are some of the predominant materials used as SLs. They have a layered structure that shears easily under sliding contact, giving rise to low coefficients of friction. The lubrication performance of MoS_2 often exceeds that of graphite and is very effective in vacuum environments. Typical fabrication of MoS_2 films includes sputtering (5), pulsed laser deposition (6), burnishing, arc evaporation, resin bonding, etc. However, MoS_2 films produced using these techniques lack the hardness needed for providing sufficient wear resistance (4). Various other strategies to circumvent this problem and to improve the tribological properties of these materials include complicated multistep processes such as alloying of MoS_2 and other SLs with a hard coating to produce a three-dimensional (3D) nanocomposite or texturing of the surface of a hard-phase material to produce pores that are subsequently filled with reservoirs of SLs (4, 7—9). One of the challenges of 3D nanocomposites for tribological applications is controlling their mechanical and tribological properties due to the codeposition of multiple (three or more) phases in the coating layers. The texturing process can be tedious and time-consuming because it requires the deposition of the hard and SL phases separately. This technique sometimes necessitates expensive fabrication pathways such as lithography, laser texturing, or plasma etching through a mask.

Recently, studies have also focused on the tribological properties of carbon nanostructures, mainly carbon nanotubes (CNTs) (10—14), which are nanometer-sized tubes of single-layer graphite (assembled either coaxially or in bundles) with outstanding mechanical, chemical, and thermal properties (15—20). CNTs are also used as fillers in base-lubricant materials to improve their frictional and wear properties (14). However, desirable results were only achieved when tedious and appropriate post-growth functionalization of the CNT surfaces was used (14). Because of the high mechanical strength of CNTs, they can provide exceptional mechanical support for SL coatings. However, investigations of the tribological behavior of pure CNT structures have shown that under high frictional load extensive graphitization of CNT surfaces occurs, thereby increasing their μ and w (10). In this paper, we report our preliminary results on an easy, reproducible, and scalable technique for producing SL coatings with superior tribological and mechanical properties compared to those presently available. We describe here the synthesis and characterization of MoS_2—CNT nanocomposite coatings and the results obtained pertaining to their frictional and wear properties. MoS_2 nanoclusters were electrochemically deposited on aligned CNTs. These nanocomposites provided extremely low μ and w under rigorous

* Corresponding authors. E-mail: pkohli@chem.siu.edu (P.K.), saouadi@physics.siu.edu (S.A.), stalapatra@physics.siu.edu (S.T.).
Received for review December 16, 2008 and accepted February 6, 2009
† Department of Physics, Southern Illinois University—Carbondale.
‡ Wright-Patterson Air Force Base.
§ Department of Chemistry and Biochemistry, Southern Illinois University—Carbondale.
DOI: 10.1021/am800240e

wear testing at room and elevated temperatures and under low- and high-humidity conditions.

MATERIALS AND METHODS

Nanotube Growth. We have used a ferrocene–xylene chemical vapor deposition (CVD) system for the growth of vertically aligned CNTs directly onto Inconel substrates. A solution containing 1 g of ferrocene in 100 mL of xylene was injected into a tube furnace maintained at 790 °C (containing the Inconel substrates) using a syringe pump (pumping speed of ~0.11 mL/min). A mixture of argon and hydrogen (85% argon) was flown at 500 sccm to carry the xylene vapors containing the catalyst before entering the furnace.

MoS_2 Deposition. Electrodeposition of MoS_2 was carried out via cathodic reduction of a 0.005 M aqueous solution of ammonium tetrathiomolybdate, $(NH_4)_2MoS_4$. Potassium chloride (KCl) with a concentration of 0.1 M was used as a supporting electrolyte. The samples were soaked in the electrolyte for 15 min prior to deposition. Potentiostatic conditions, with a current density of 8.32 mA/cm^2, were maintained for 15 min using a Sorenson power supply. The samples were then dried in argon and were subsequently prepared for wear testing.

Wear Testing and Measurements. Wear testing was performed using a Nanovea tribometer (Microphotonics, Irvine, CA). Ball-on-disk tests were performed in a dry air environment, with a relative humidity of 0.1%, using a 1 N load and a rotational speed of 200 rpm. Alumina Al_2O_3 balls with diameters of 6 mm were employed as counterface materials. The coatings were allowed to run until failure. Characterization of the wear tracks was carried out using a Nanovea optical profilometer (Microphotonics, Irvine, CA). The wear loss and normalized w were determined from the cross section of the wear track, measured using multiple-surface profilometry. The formula used to calculate w is $w = \pi DA/NL$, where w is the wear rate expressed in mm^3/N · mm, D is the diameter of the wear track in mm, A is the cross-sectional area of the wear track in mm^2, N is the normal applied load, and L is the total sliding distance during the wear test in m.

Microscopy. Scanning electron microscopy (SEM) was performed on the as-produced samples using a Hitachi S570 scanning electron microscope. For transmission electron microscopy (TEM), the CNT–MoS_2 composite was scraped off of the Inconel disk and sonicated in an alcohol solution (for 5 min). The alcohol solution containing the composite material was deposited on lacey carbon TEM grids for microscopy and diffraction experiments.

RESULTS AND DISCUSSION

The procedure used for fabricating the CNT–MoS_2 SL composites is shown in Figure 1. Aligned CNT films were grown directly on a polished Inconel 600 disk of 1 in. diameter using floating-catalyst CVD reported earlier (21) (see the Materials and Methods section). The CNTs grown using this process are known to adhere well onto the Inconel surface (21). These disks were directly used as electrodes for the electrodepositon of MoS_2 using an aqueous 5 mM $(NH_4)_2MoS_4$ solution with 0.1 M KCl as the supporting electrolyte under potentiostatic conditions for 15 min. Figure 1a schematically shows the synthesis of CNT–MoS_2 composites. To check the morphology and the form of the electrodeposited materials, detailed electron microscopy characterization of the samples was performed. In Figure 1b, a high-magnification SEM image of CNT–MoS_2 composites is shown. The figure indicates that the process of electrodeposition results in the formation of MoS_2 clusters on

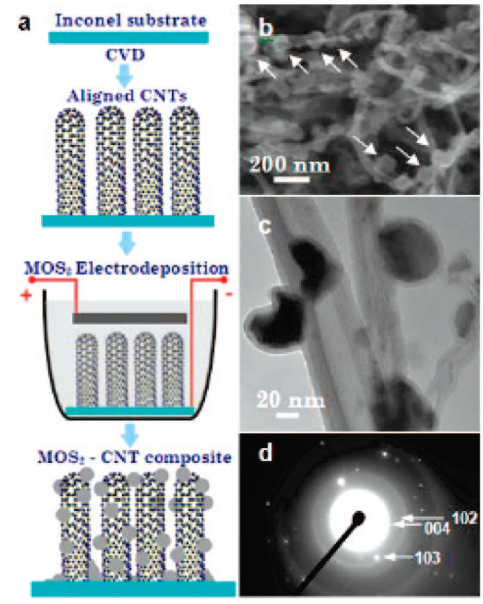

FIGURE 1. Schematics of the fabrication and electron microscopy characterization of aligned multiwall nanotube–MoS_2 composites grown on Inconel. (a) Schematic showing the various steps involved in the fabrication of CNT–MoS_2 composites. (b) High-magnification SEM image of CNT–MoS_2 composites. Note the site-specific attachment of MoS_2 clusters on the CNT surfaces (shown by the arrows). (c) Selected-area TEM image showing well-adhered clusters on CNT surfaces. (d) Electron diffraction pattern from the CNT–MoS_2 composites. The diffraction spots shown correspond to the diffraction from MoS_2 crystal planes. The diffraction rings in the image are due to the presence of carbon (see the Supporting Information for details of this image).

the CNT surfaces. Owing to the low temperatures used in the CVD technique, the CNTs are expected to possess some inherent surface defects. These defects have enhanced electric fields in their vicinity when used as an electrode in an electrochemical bath and act as nucleation sites for MoS_2 nanocluster formation. The diameters of the MoS_2 nanoparticles deposited on CNTs are ~40–90 nm. In Figure 1c, a TEM image of a small portion of the composite is shown. Formation of MoS_2 clusters on CNT surfaces is also evident from this image. The clusters were well adhered to CNT surfaces, and they remained intact with CNTs after ultrasonic agitation treatment for 1–2 h. In Figure 1d, an electron diffraction pattern obtained from a selected area of the CNT–MoS_2 composite is shown. The diffraction pattern shows random diffraction spots indicating the polycrystalline nature of the electrodeposited MoS_2. Some of these spots were indexed and correspond to (103), (102), and (004) MoS_2 crystal planes. Details of the indexing and the corresponding D values are presented in the Supporting Information.

The results of the tribological measurements on these composite films are presented in Figure 2. Ball-on-disk tests were performed to determine μ and w of the CNT–MoS_2 composites in a dry air environment, with a relative humidity of 0.1%, using a 1 N load (average contact pressure of 0.5 GPa) and a rotational speed of 200 rpm. The alumina test balls of 1 mm diameter were used for these experiments. The wear track resulting from the ball-on-disk measurements performed on CNT–MoS_2 composite films of ~20

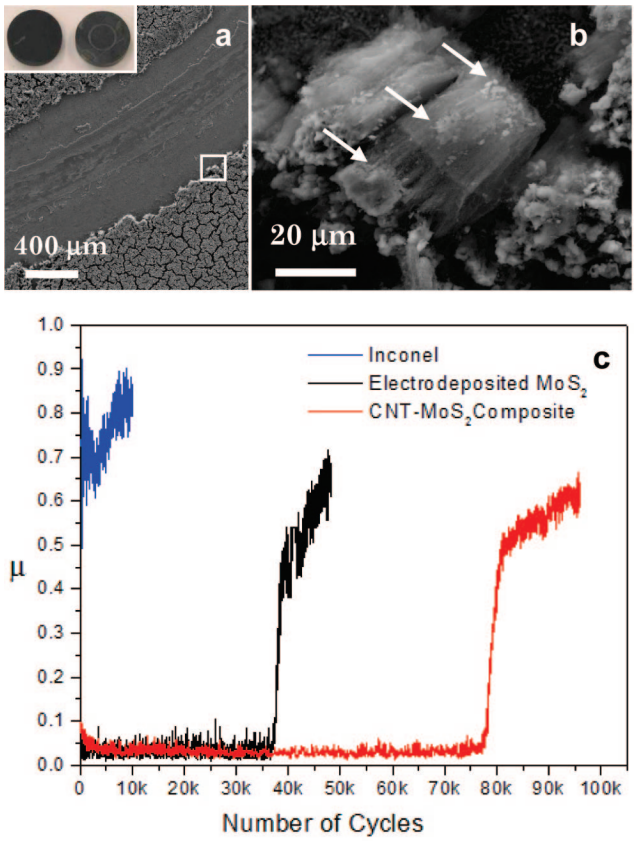

FIGURE 2. Wear test on CNT−MoS_2 composite films. (a) Top surface and the wear track resulting from tribological measurements performed on the CNT−MoS_2 films grown on Inconel. Inset: as-produced aligned CNT film on an Inconel disk (left) as well as MoS_2-coated CNT films after wear measurement (right). The circular wear track is also visible on the film. The disks are 1 in. in diameter. (b) High-magnification image (of the region marked by a white square in part a) of debris formed in the vicinity of the wear track due to the friction measurement. Here we note that deposition of MoS_2 has occurred throughout the length of the CNTs. The arrows on the top, middle, and the bottom of the peeled-off aligned CNT bundles show the obvious MoS_2 deposition. (c) Friction coefficient (y axis) measured on a bare Inconel disk, electrodeposited MoS_2, and a CNT−MoS_2 composite film plotted as a function of the number of wear cycles (x axis). k in the legend indicates a thousand. The data indicate low μ and the long life of the CNT−MoS_2 composite film.

μm thickness is shown in Figure 2a. In Figure 2b, a magnified view of debris peeled at the edge of the track during the wear test shows bundles of aligned CNT−MoS_2 composites. It is evident from the image that, although the lengths of the CNTs are ∼20 μm, deposition of MoS_2 is not restricted to the tips of the CNTs, but it occurs throughout the length of the CNT bundles. Figure 2c shows the friction coefficients and life cycle of the CNT−MoS_2 composites. For a precise estimation of the enhanced tribological properties of the CNT−MoS_2 composites, we performed measurements on reference samples prepared by electrodepositing MoS_2 on bare Inconel substrates under the same experimental conditions as those for CNT-coated Inconel samples. The MoS_2 reference coating also exhibited $\mu = 0.04$ (Figure 2c), which is typical for this material. This is because MoS_2 has a layered structure in which vicinal sulfur layers are bound by van der Waals forces that shear easily under an applied load, exhibiting a low friction coefficient. These coatings were not robust, and they failed after tribotesting for about 35 000 (35K)

Table 1. Results of Tribological Tests on Various SL Films

sample	temp (°C)	μ	w (mm^3/N · mm)
bare Inconel	25	0.75	5.8×10^{-7}
electrodeposited MoS_2 film	25	0.04	4.1×10^{-10}
CNT film[a]	25	0.2,[a] 0.090−0.795[b]	
CNT−MoS_2 film (I)	25	0.03	3.1×10^{-13}
CNT−MoS_2 film (I) (repeat)	25	0.03	3.1×10^{-13}
CNT−MoS_2 film (II)	25	0.03	6.0×10^{-12}
electrodeposited MoS_2 film	300	0.05	1.9×10^{-8}
CNT−MoS_2 film (I)	300	0.07	8.0×10^{-12}
sputtered MoS_2 (1)	25	0.1−0.3	$\sim 3.0 \times 10^{-9}$
nanoparticles MoS_2 (1)	25	0.008−0.01	$\sim 1.0 \times 10^{-11}$

[a] Hu, J. J.; Jo, S. H.; Ren, Z. F.; Voevodin, A. A.; Zabinski, J. S. *Tribol. Lett.* **2005**, *19*, 119−125. [b] Dickrell, P. L.; Sinnott, S. B.; Hahn, D. W.; Raravikar, N. R.; Schadler, L. S.; Ajayan, P. M.; Sawyer, W. G. *Tribol. Lett.* **2005**, *18*, 59−62.

cycles. We estimated a w value of $\sim 10^{-10}$ mm^3/N · mm for MoS_2-coated Inconel samples by characterizing the tracks using optical profilometry (see the Materials and Methods section). Under the same experimental conditions, the CNT−MoS_2 composite films, however, were found to be much more robust and showed much higher frictional and wear properties. To check the repeatability and validity of the measurements and results, tests were also performed at various locations of the CNT−MoS_2 nanocomposite Inconel disks as well as on multiple samples. μ and w of all of the samples were found to be within the 0.03−0.04 and 8.1 $\times 10^{-12}$−3.1 $\times 10^{-13}$ mm^3/N · mm ranges, respectively. For comparison, w values obtained for our samples are about 4 orders of magnitude smaller than those measured on sputtered MoS_2 films (1) and about 2 orders of magnitude smaller than those measured on the nanoparticle MoS_2 films (1) (see Table 1).

We attribute the enhanced tribological properties of these composites to the following reasons. First, CNTs can withstand high compressive loads without fracture or collapse over many cycles (18). Thus, the high resilience of the CNTs under extreme loads provides a "cushioning" effect to the MoS_2 nanoclusters. The recovery of the CNT films to their original form, once the compressing load is released, is also very fast (almost instantaneous) (18), making the process of compressive deformation and subsequent recovery somewhat elastic in nature. Furthermore, some energy involved in the frictional studies will also be dissipated because of the elastic nature of the MoS_2−CNT nanocomposites. This, in turn, makes the CNT−MoS_2 composites strong load-bearing materials with enhanced frictional and wear properties.

Additionally, evidence of reduced surface activity toward oxidation of the MoS_2 clusters attached on the CNT surfaces was also observed from Raman measurements (Supporting Information). The lower-wavenumber region of the Raman spectra obtained from the as-deposited CNT−MoS_2 film as well as from the wear track showed peaks in the 200−1000

cm^{-1} region. In this region, the peaks are typically associated with both MoS_2 (22, 23) and molybdenum oxide (MoO_3) (24, 25). The presence of Raman peaks in the 870−966 cm^{-1} region indicated MoS_2 oxidation for the CNT−MoS_2 portion that was exposed to air. The intensities of the peaks in the 870−966 cm^{-1} regions of the films in the wear tracks were significantly reduced compared to those of the spectrum taken from the top of the coating. Moreover, the peaks in the 1400−1600 cm^{-1} region associated with CNTs remained relatively constant for spectra taken at the center of the wear track and the top surface, suggesting that the CNT contents in these regions are probably constant. Collectively, these spectroscopic observations indicate that the decreased MoO_3 concentration in the wear track region compared well to that in the top of the SL coating. It is possible that the reduced oxidation behavior of MoS_2 nanoclusters, once supported on CNT surfaces, could also be a contributing factor for the enhanced frictional and wear properties.

We examined the effect of incorporating a CNT−MoS_2 SL on the frictional properties of commercial machine oil. A total of 3 mg of CNT−MoS_2 was mixed with commercial machine oil in an ultrasonic bath. Repeated sonication cycles were performed to obtain a well-dispersed CNT−MoS_2−oil solution. Friction tests (up to 1000 cycles with 1 N load) were performed on as-received machine oil as well as the prepared suspension (a few drops of the fluids were dropped on polished Inconel). We found that μ of the MoS_2−CNT−machine oil system was reduced ~15% from ~0.095 to ~0.081 because of the presence of CNT−MoS_2 (see the Supporting Information). This shows the ability of the CNT−MoS_2 nanocomposites to enhance the tribological properties of commercial liquid lubricants. These sets of experiments clearly demonstrate the possibility of enhancing the tribological properties of liquid lubricants with nanocomposite SLs added. We believe that with optimization of the experimental conditions both μ and w for a MoS_2−CNT−oil suspension can be further improved.

From an application point of view, the use of some of the SLs is severely restricted by the operating conditions. For example, the operating temperature for poly(tetraefluoroethylene) (Teflon)-based lubricants is limited to ~250 °C (1b). Similarly, the tribological properties (mainly w and, hence, the life cycle) of MoS_2 films at elevated temperatures (~400 °C) deteriorate rapidly because of its oxidation to MoO_3 (1b). Furthermore, very few studies on the tribological properties of CNT coatings have been reported. One such study showed that the friction coefficient varied from a high value of 0.795 for vertically aligned CNTs of 50 μm length to a very low value of 0.09 for the CNTs dispersed flat on substrates (26). Another study included the deposition of vertically aligned CNT arrays as thin films on 440 °C stainless steel substrates by plasma-enhanced CVD at a moderately low deposition temperature (27). $\mu \sim 0.2$ was measured in all humid air tribotests. A low coefficient of friction was only measured under a load of 10 g in dry nitrogen, while a much higher value of the coefficient of friction was measured under loads of 25 and 100 g. SEM observations showed that the CNTs were pushed down into a horizontal position by rubbing. The CNTs clumped together and were then compressed, which resulted in the formation of graphite-like carbon films. Our CNT−MoS_2 films, on the other hand, showed extremely low μ and w of 0.03−0.04 and 8.1 × 10^{-12}−3.1 × 10^{-13} $mm^3/N \cdot mm$ ranges, respectively, under low humidity and room temperature using a 100 g load. We also investigated the frictional properties of our CNT−MoS_2 nanocomposite coatings at high humidity (50%). The coatings performed well at 50% relative humidity and showed $\mu \sim 0.1$ under these conditions. Collectively, these experiments show that CNT−MOS_2 nanocomposite coatings have potential uses where the applications demand superior tribological and frictional properties under a variety of conditions.

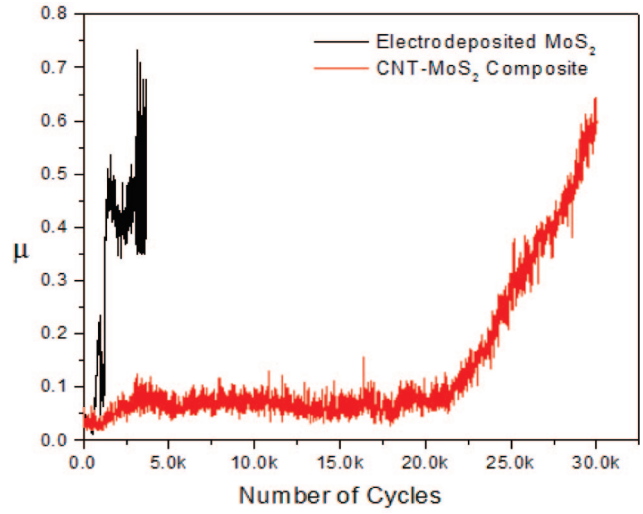

FIGURE 3. High-temperature wear test of a CNT−MoS_2 composite. μ (y axis) measured at 300 °C on a bare Inconel disk, an electrodeposited MoS_2, and a CNT−MoS_2 composite film plotted as a function of the number of wear cycles (x axis). k in the legend indicates a thousand. The material wear life was improved by a factor of ~4 while maintaining reduced μ.

To investigate the high-temperature tribological properties of our coatings, friction tests were performed on electrodeposited MoS_2−Inconel and CNT−MoS_2−Inconel substrates at 300 °C. The results are shown in Figure 3. We found that the electrodeposited MoS_2 films on Inconel failed within a few thousand cycles (μ increased from ~0.04 to ~0.45) of tribological testing at elevated temperature whereas the CNT−MoS_2 coatings were stable under similar frictional testing conditions for >22K cycles. These results clearly demonstrate that at relatively high temperatures the wear reduction was drastically improved for CNT−MoS_2 coatings compared to bare MoS_2 coatings. The enhanced tribological properties of MoS_2−CNT coatings are attributed to (1) the extremely high thermal conductivity of the CNTs (19, 20), which prevent localized heating of the MoS_2 clusters by quickly dissipating the heat within the CNT matrix and thereby delaying the oxidation process of MoS_2, and (2) reduced MoS_2 oxidation when incorporated in CNTs.

In conclusion, we synthesized MoS_2−CNT high-performance lubricant materials by electrodepositing MoS_2 on

CNT-containing Inconel substrates. These materials provided excellent tribological properties at both room and elevated temperatures. The ease of this fabrication process will allow large-scale production of these materials. Although our results are specifically shown for MoS_2—CNT SLs, we anticipate that this method can be extended to the synthesis of similar CNT-based SLs using a diverse group of materials such as WS_2, WSe_2, and silver. This will open up many possibilities of fabricating SLs with tailored properties that are suitable for tribological applications under different experimental conditions.

Acknowledgment. S.T. acknowledges start-up funding support received from SIUC's Office of Research Development and Administration. P.K. acknowledges the NSF (CAREER Award and CMMI 0653986), and S.A. thanks the NSF (CMMI 0653986) and the U.S. Department of the ARMY (Award W911NF-08-1-0460) for partial funding of this work.

Supporting Information Available: Information on the low-magnification TEM image of a CNT—MoS_2 composite (Figure S1), calculated *d* values and *hkl* planes from TEM diffraction of a CNT—MoS_2 composite (Table S1), Raman spectra measured from the top surface of the as-deposited film and the wear track of a CNT—MoS_2 film (Figure S2), friction measurements on an as-received commercial machine oil and emulsion prepared from commercial machine oil and CNT—MoS_2 composites (Figure S3). This material is available free of charge via the Internet at http://pubs.acs.org.

REFERENCES AND NOTES

(1) (a) Chhowalla, M.; Amaratunga, G. A. J. *Nature* **2000**, *407*, 164–167. (b) Marina, G. In *Lubricant Additives: Chemistry and Applications*; Rudnick, L. R., Ed.; Taylor and Francis: New York, 2007.
(2) Rapoport, L.; Bilik, Y.; Feldman, Y.; Homyonfer, M.; Cohen, S. R.; Tenne, R. *Nature* **1997**, *387*, 791–793.
(3) Zabinski, J. S.; Sanders, J. H.; Nainaparampil, J.; Prasad, S. V. *Tribol. Lett.* **2000**, *8*, 103.
(4) Erdemir, A. *Tribol. Int.* **2005**, *38*, 249–256.
(5) Liu, Y. R.; Liu, J. J.; Du, Z. *Wear* **1999**, *231*, 285–292.
(6) McDevitt, N. T.; Bultman, J. E.; Zabinski, J. S. *Appl. Spectrosc.* **1998**, *52*, 1160–1164.
(7) Aouadi, S. M.; Paudel, Y.; Luster, B.; Stadler, S.; Kohli, P.; Muratore, C.; Hager, C.; Voevodin, A. A. *Tribol. Lett.* **2008**, *29*, 95.
(8) Basnyat, P.; Luster, B.; Muratore, C.; Voevodin, A. A.; Haasch, R.; Zakeri, R.; Kohli, P.; Aouadi, S. M. *Surf. Coat. Technol.* **2008**, *203*, 73–79.
(9) Moshkovith, A.; Perfiliev, V.; Gindin, D.; Parkansky, N.; Boxman, R.; Rapoport, L. *Wear* **2007**, *263*, 1467.
(10) Hu, J. J.; Jo, S. H.; Ren, Z. F.; Voevodin, A. A.; Zabinski, J. S. *Tribol. Lett.* **2005**, *19*, 119–125.
(11) Dickrell, P. L.; Pal, S. K.; Bourne, G. R.; Muratore, C.; Voevodin, A. A.; Ajayan, P. M.; Schadler, L. S.; Sawyer, W. G. *Tribol. Lett.* **2006**, *24*, 85–90.
(12) Miyoshi, K.; Street, K. W., Jr.; Vander Wal, R. L.; Andrews, R.; Sayir, A. *Tribol. Lett.* **2005**, *19*, 191–201.
(13) Xia, Z. H.; Loub, J.; Curtin, W. A. *Scr. Mater.* **2008**, *58*, 223–226.
(14) Pei, X.; Liu, W.; Hao, J. *J. Polym. Sci., Part A: Polym. Chem.* **2008**, *46*, 3014–3023.
(15) Dresselhaus, M. S.; Dresselhaus, G.; Avouris, P. Carbon Nanotubes: Synthesis, Structure, Properties and Applications. *Topics in Applied Physics*; Springer: Heidelberg, Germany, 2001.
(16) Ajayan, P. M. *Chem. Rev.* **1999**, *99*, 1787–1800.
(17) Cao, A.; Vinod, V.; Li, X.; Yao, Z.; Ghasemi-Nejhad, M.; Ajayan, P. M. *Nat. Mater.* **2005**, *4*, 540–545.
(18) Cao, A.; Dickrell, P. L.; Sawyer, W. G.; Ghasemi-Nejhad, M. N.; Ajayan, P. M. *Science* **2005**, *310*, 1307–1310.
(19) Hone, J. Carbon Nanotubes: Thermal Properties. *Dekker Encyclopedia of Nanoscience and Nanotechnology*; Marcel Dekker Inc.: New York, 2004; pp 603—610.
(20) Kim, P.; Shi, L.; Majumdar, A.; McEuen, P. L. *Phys. Rev. Lett.* **2001**, *21*, 215502.
(21) Talapatra, S.; Kar, S.; Pal, S.; Vajtai, R.; Ci, L.; Victor, P.; Shaijumon, M. M.; Kaur, S.; Nalamasu, O.; Ajayan, P. M. *Nat. Nanotechnol.* **2006**, *2*, 1–5.
(22) McDevitf, N. T.; Zabinski, J. S.; Donley, M. S.; Bultman, J. E. *Appl. Spectrosc.* **1994**, *48*, 733–736.
(23) Frey, G. L.; Tenne, R.; Mattews, J. M.; Dresselhaus, M.; Dresselhaus, G. *Phys. Rev. B* **1999**, *60*, 2883–2892.
(24) Atuchin, V. V.; Gavrilova, T. A.; Kostrovsky, V. G.; Pokrovsky, L. D.; Troitskaia, I. B. *Inorg. Mater.* **2008**, *44*, 622–627.
(25) Krishnan, C. V.; Chen, J.; Burger, C.; Chu, B. J. *Phys. Chem. B* **2006**, *110*, 20182–20188.
(26) Dickrell, P. L.; Sinnott, S. B.; Hahn, D. W. *Tribol. Lett.* **2005**, *18*, 59–62.
(27) Hu, J. J.; Jo, S. H.; Ren, Z. F.; Voevodin, A. A.; Zabinski, J. S. *Tribol. Lett.* **2005**, *19*, 119–125.

AM800240E